von Zeipel effect visited by interferometry

Armando DOMICIANO de SOUZA Jr & Farrokh VAKILI

(Observatoire de la Côte d'Azur - GI2T/ISA - France)

Abstract

The von Zeipel effect is supposed to be present in rapidly rotating stars resulting in poles hotter and brighter than the equator. Previous interferometric observations of the rapidly rotating star Altair have already been performed by Hanbury Brown with the Narrabri interferometer (Hanbury Brown 1974) which did not have the required sensibility to allow a suitable identification of stellar parameters. This sensibility can be attained by present modern interferometers.

Townsend's non-radial pulsation (NRP) (Townsend 1997) model have been adapted in order to simulate the photocenter shifts curves and intensity maps for fast rotating stars. In addition, Hubeny's radiative transfer code TLUSTY/SYNSPEC (Hubeny 1988 and Hubeny&Lanz 1995) was used to synthesize the photospheric local spectrum.

Interferometry Summerschool, Leiden - The Netherlands, September 18-22, 2000

1.1 Introduction

Physical model

The physical model adopted here is summarized in figure 1.1. We may distinguish two main parts which produce:

1. Synthetic spectra (codes TLUSTY and SYNSPEC; Hubeny 1988 and Hubeny&Lanz 1995):

   (a) TLUSTY: calculates plane-parallel, horizontally homogeneous model stellar atmospheres in radiative and hydrostatic equilibrium as a function of temperature (T), gravity (g), chemical abundance, etc.

   (b) SYNSPEC: calculates the emergent spectrum (local specific intensity) from a given model atmosphere.

2. Stellar surface structures (codes BRUCE and KYLIE; Townsend 1997)

   (a) BRUCE: calculates a discrete photospheric stellar model (local values of temperature, gravity, velocity field, projected surface areas, etc).

   (b) KYLIE: calculates the disc integrated spectra from the outputs of BRUCE and SYSNPEC. We modified the original KYLIE in order to calculate differential stellar photocenters (photometric centeroid) and intensity maps as a function of wavelength.
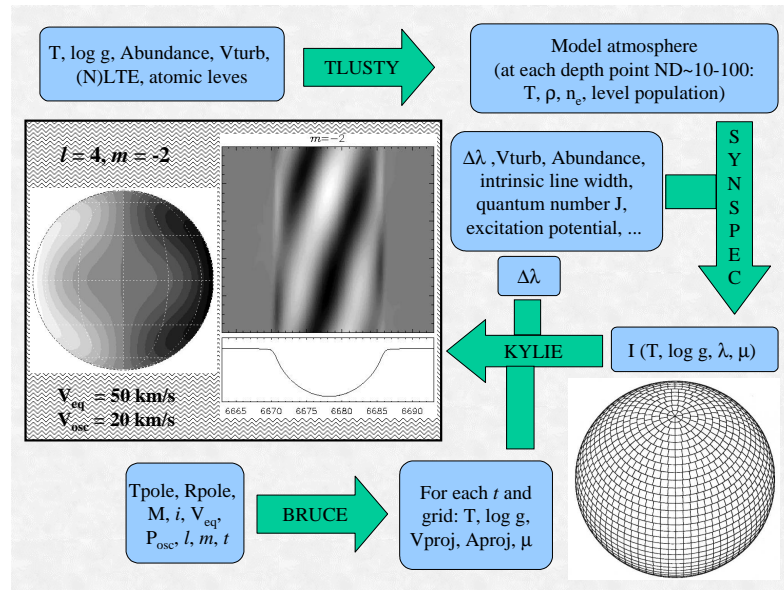

FIG. 1.1: Synoptic diagram of the physical model adopted in this work.

Spectra and photocentres

The spectra F_{obs} and photocenters $\vec{\epsilon}$ result from the integral of the specific intensity I over the stellar disc (double numerical summation) by using the following relations:

$$
\begin{aligned}
F_{\text{obs}}(\lambda) &= \int I(\lambda, \omega)\mathrm{d}\omega = \int I(\lambda, S_{\text{proj}})\frac{\mathrm{d}S_{\text{proj}}}{D^2} = \\
&= \int\int I(\lambda, x, y)\frac{\mathrm{d}x\mathrm{d}y}{D^2}
\end{aligned}
\tag{1.1}
$$

and

$$
\vec{\epsilon}(\lambda) = \epsilon_x(\lambda)\widehat{i} + \epsilon_y(\lambda)\widehat{j}
\tag{1.2}
$$

where

$$
\epsilon_i(\lambda) = \frac{\int\int iI(\lambda, x, y)\,\mathrm{d}x\mathrm{d}y}{\int\int I(\lambda, x, y)\,\mathrm{d}x\mathrm{d}y} = \frac{\int\int iI(\lambda, x, y)\,\mathrm{d}x\mathrm{d}y}{D^2 F_{\text{obs}}(\lambda)}\; ; \;\; i = x, y
\tag{1.3}
$$

>From equations 1.1 to 1.3 D is the stellar distance, S_{proj} is the elementary surface projected towards the observer and variables x and y are defined by the reference system shown in figure 1.2.
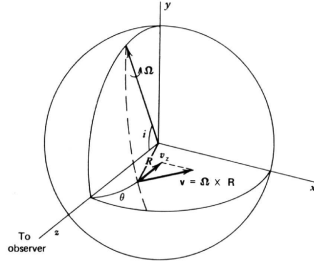

FIG. 1.2: Reference system adopted for the intensity maps, spectra and photocenter calculations. The projected stellar disc is located in the plan xy (image from Gray 1992).

von Zeipel effect

By adopting a simple model of a rotationally distorted star one can obtain the von Zeipel result (von Zeipel 1924) which states that local flux (and thus the local effective temperature) is proportional to the local effective gravity. This is translated in a gravity darkening law of the form:

$$
T(\theta) = T_{\text{pôle}}\left(\frac{g(\theta)}{g_{\text{pôle}}}\right)^{\beta}
\tag{1.4}
$$

For the photosphere of early-type stars an appropriate value of beta is 0.25 (Townsend 1997 and von Zeipel 1924). The physical model described above includes this gravity darkening law.

1.2   Simulation results

We present here our simulations of the consequences of the von Zeipel effect on stellar spectra and photocentres. As an example the table 1.1 shows the adopted parameters for a theoretical rapidly rotating early-type star (hereinafter called "von Zeipel" star).

TAB. 1.1: Parameters adopted for the study of the von Zeipel effect.

Free parameters	Derived parameters
$M = 15$ M$_\odot \Rightarrow \log g_{\mathrm{pole}} = 4.06$ dex	$\log g_{\mathrm{eq}} = 3.79$ dex
$R_{\mathrm{pole}} = 6$ R$_\odot$	$R_{\mathrm{eq}} = 6.86$ R$_\odot \Rightarrow R_{\mathrm{pole}} = 87\% R_{\mathrm{eq}}$
$T_{\mathrm{pole}} = 30000$ K	$T_{\mathrm{eq}} = 25763$ K
$v_{\mathrm{eq}} = 346.41$ km/s	$v_{\mathrm{eq}} = 61.5\% v_{\mathrm{crit}}$
$i = 60°$	$v_{\mathrm{eq}} \sin i = 300$ km/s
Number of equatorial grids $= 1000$	Number of visible grids $= 159287$
Without NRP	
Spectra from TLUSTY/SYNSPEC	
Spectral region around HeI $\lambda6678$	

Figure 1.3 is the temperature map for this star where we note the visible pole, hotter and brighter than the equator, which shifts the photocentre position towards itself. Such effect is more easily seen in figure 1.4 which shows a comparison between the spectra and photocentres for the "von Zeipel" star and for a homogeneous spherical star with identical physical parameters (table 1.1). The photocentre coordinates ϵ_x are similar and their form reflects the consequences of the stellar rotation on the photocentre shifts measured inside absorption lines (Doppler imaging effect). On the other hand, ϵ_y for the "von Zeipel" star is globally displaced towards the visible pole ($\sim 3\%$ Req) while for the spherical homogeneous star $\epsilon_y = 0$ as expected. Note also that inside the line profile ey for the "von Zeipel" star shows a small ($\sim 0.1\%$Req) differential effect when compared to the continuum. Finally, the spectra of both models are similar with small discrepancies caused mostly by the different temperature distribution.

1.3   Conclusions and perspectives

The example presented in this work shows that the "von Zeipel" theorem can be studied by the utilization of modern optical interferometers (spatial resolution $\lesssim 1$ mas). Previous interferometric observations of the rapidly rotating star Altair have already been performed by Hanbury Brown with the Narrabri interferometer (Hanbury Brown 1974) where a significant stellar radius deformation was detected. However, the Narrabri interferometer did not have the required sensibility to allow a suitable identification of stellar parameters.

The required sensibility can be attained by more modern interferometers which are (or will be) able to apply techniques like the Differential Speckle Interferometry (DSI, Beckers 1982). The DSI allows photocentre measurements with a spatial resolution better than
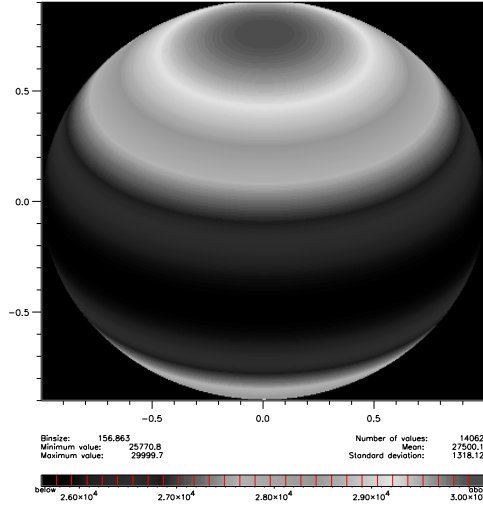
FIG. 1.3: Temperature map for the "von Zeipel" star (table 1.1). The temperature difference between the poles and the equator is about 4000K which shifts the photocentre from the central region (sub-observers latitude) towards the visible pole.
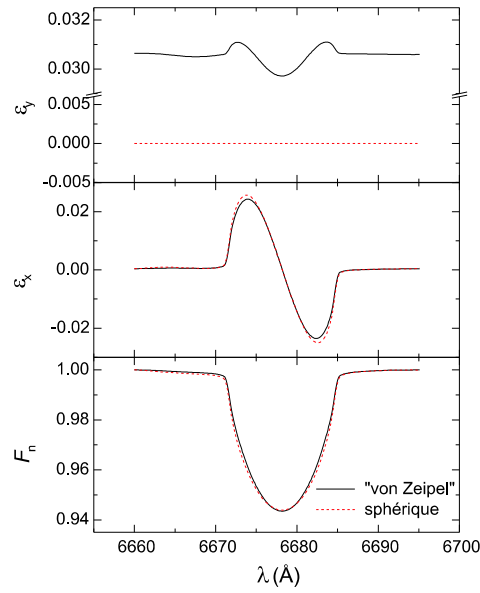

FIG. 1.4: Normalized spectra and photocentres ϵ_x and ϵ_y (stellar radii units) simulated for the "von Zeipel" star (solid) and for a spherical star with identical input parameters (dashed). The biggest difference is shown by ϵ_y which is globally displaced towards the visible pole.

5

the diffraction limit, consiting thus a powerful tool for the study of photospheric stellar structures (Vakili&Percheron 1990 and Lagarde 1994). Some instruments like PRIMA (Delplancke et al.2000) will also work with a reference for the phase variations of the studied star, allowing precise measurements even when photocentre is globally (continuum + line) displaced.

In the future, we will perform a more deep study of these effects in order to 1) establish the correct instrumentals/sensibility requirements for the observations and 2) to develop an optimized method of observation and data analysis for recovering the desired stellar parameters. We will also perform a study of the consequences of rapid stellar rotation on visibility curves.

1.4 Acknowledgements

1.5 References

Beckers, J.M. 1982, Opt.Acta, 29, 361

Delplancke, F., Lévêque, S., Kervella, P., Glindemann, A. and d'Arcio, L. "Phase-referenced imaging and micro-arcsecond astrometry with the VLTI," in *Interferometry in Optical Astronomy*, P.Léna, ed., Proc.SPIE 4006, 2000

Gray, D.A. *The observation and analysis of stellar photospheres.* Cambridge University Press, 1992

Hanbury Brown, R. *The Intensity Interferometer.* Taylor & Francis Ltd, London, 1974

Hubeny, I. 1988, Comp.Phys.Comm., 52, 103

Hubeny, I. and Lanz, T. 1995, ApJ, 439, 875

Lagarde, S. 1994, PhD thesis, Université de Nice-Sophia Antipolis

Townsend, R.H.D. 1997, MNRAS, 284, 389

Vakili, F. and Percheron, I., in *Rapid Variability of OB-Stars: Nature and Diagnostic Value*, D.Baade, ed., 1990

von Zeipel, H. 1924, MNRAS, 84, 665

Differential Interferometry at VLTI for direct detection of hot exoplanets

M. Vannier[1], R. Petrov[1] , B. Lopez[2]

[1] Laboratoire d'Astrophysique de l'UNSA, Nice, France
[2] Observatoire de la Cote d'Azur, Nice, France

A differential interferometric method using the Amber and Midi instruments of the VLTI, consisting in simultaneous measurements of fringe phase and visibility between two wavelengths, is proposed to detect hot Jupiter-like exoplanets. Current estimations on SNR indicate the potential of such detection with apropriate calibration procedures. In addition to direct detection, the resolution of spectral features in the planetary atmosphere should be feasable, thus constraining the models on exoplanets.

Introduction: For the past 5 years, nearly 50 extrasolar planets have been found by measuring induced radial velocity variations or during a photometric occultation of the star by its companion. Direct detection of a planet with current instruments, though, is considerably more difficult because of the very high luminosity ratio betwen the two components, which requires an accuracy on visibility of about 10^{-5} to distinguish the planetary signal from the star. Such a level of precision cannot be reached on absolute by traditional interferometry. We propose to overcome this by using a relative method called Differential Interferometry.

Interferometry with dispersed fringe
On the VLTI, the Amber and Midi instruments will perform multiaxial interferometry with a typical baseline of about 100m, and give an interferometric resolution of about 4 mas at 2 μm (Amber) and 20 mas at 10 μm (Midi), enough to resolve most known planetary systems.
Here is shown the principle of these instruments used in dispersed modes : After spatial filtering, the beams are combined, and dispersed through a slit. A photometric channel is taken from the input beams for calibration.

(figure not attached)

Differential interferometry (D.I.) consists in comparing the fringe phases ϕ and/or visibilities V simultaneously bewween different spectral channels. It measures the displacement of the photocenter with wavelength and takes advantage, in the present case, of the strong difference in color between the star and its planetary companion.

This method, as it operates in a wavelength-relative mode, is in principle not affected by the achromatic piston induced by the instrument or the atmosphere. It is combined to a spatial filtering which supresses all the higher orders of perturbations. Therefore, I.D. is only sensitive, in addition to the fundamental noises, to the wavelength-dependent OPD which is much less dominant in the interferometric biases budget. This should increase by several orders of magnitude the dynamic sensitivity with respect to « absolute » interferometric methods.
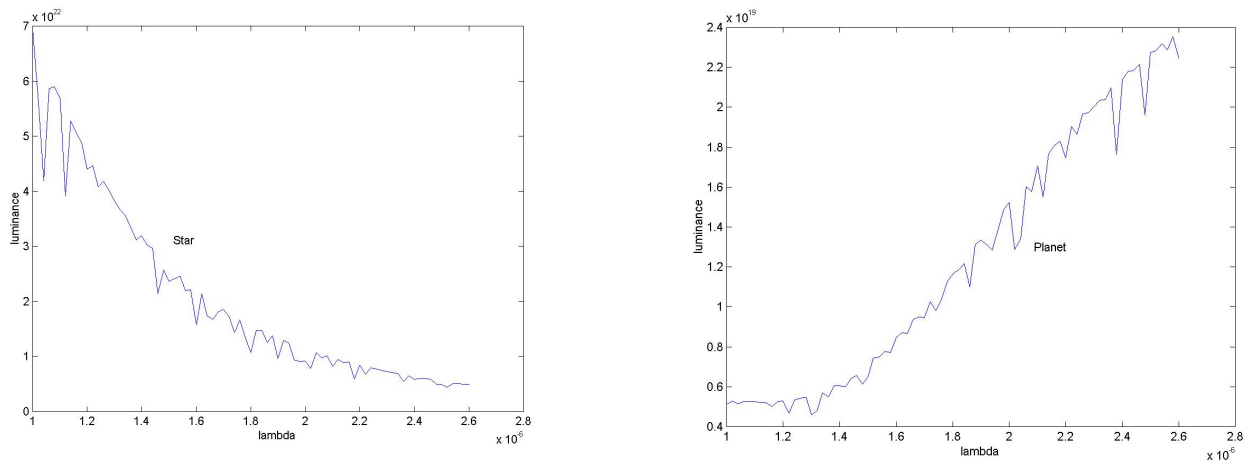
*Comparative behaviour of the spectra from a star and a planetary companion with a temperature of about 1000K. The **luminosity ratio** I*(λ)/Ipl(λ) between the components, although very high whatever the wavelength, it shows a clear variation with λ, due, at a first order, to the difference in temperature between the two bodies.*
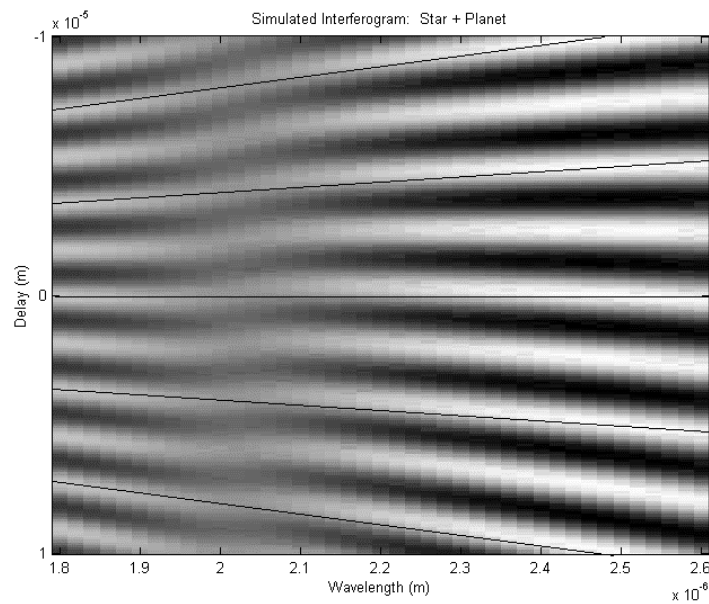
Simulated interferogram showing the dispersed fringe patterns as a fonction of OPD x against the wavelength λ. The presence of a planet (exaggerated here) is detectable by comparing phases and visibilities for different λ. Straight lines are shown here as a reference on the fringes. Actual measurements will be considerably more noisy, and the weak planetary signature will require careful calibrations.

Differential comparison of phases and visibilities should yield an unambiguous signature of a planetary companion. According to present estimations, the **noise levels of AMBER and MIDI** allow good enough SNR for detecting planets of several existing systems . **Spectral absorption** features from the planetary atmosphere are also potentially detectable on the interferogram. Depending on the observation bandwidth and on the SNR, the spectral resolution of such features could constraint some parameters of current planetary models, such as temperature, pressure, albedo, chemical composition of atmosphere,…
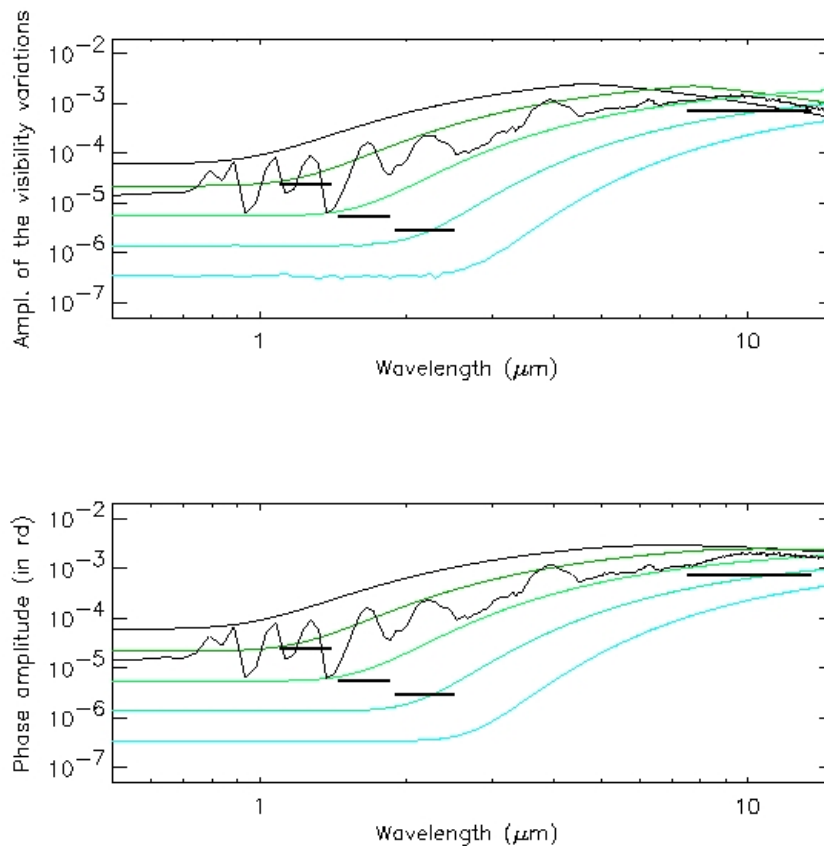
Expected fundamental noise levels for Amber and Midi on measurements of phase and visibility amplitude, at resolution 25 (about 0.1 mm in K band) and a baseline = 80 m, compared with a synthetic spectrum of 51 Peg b (Gouquenleuqe et al.) , and various « black body » planets of $1.4M_{jup}$ orbiting a star at 10pc.

The **angular separation** between the two bodies can in principle be resolved by the VLTI for most maximal separations in known planetary systems. Measurement of visibilities will constraint the geometry of such systems, whereas the measurement of phase with the

differential method gives information on the position of photocentre even for unresolved systems (e.g. at orbital phase when angular separation appears very low). Measuring separations at different times using different baselines, yields the semi-axis and the inclinaison angle unambiguously.

Correction of chromatic biases : The error budget used in fig. , though, only takes into account the fondamental noises of the system: photon, readout and thermal noises. The interferometric signal is actually further degraded by the chromatic dispersion through all the (atmospheric and instrumental) transmissive elements crossed by each of the beams. It is important to estimate and optimize the different contributions to chromatic OPD along the instrumental chain in order to apply apropriate compensation, calibration or correction procedures.

If $\rho_A(\lambda_1)$ quotes the optical path along beam A at wavelength (λ_i), the chromatic $\Delta OPD(\lambda_1, \lambda_2)$ between two beams over an interval $[\lambda_1, \lambda_2]$ writes :

$$\Delta OPD(\lambda_1, \lambda_2) = OPD(\lambda_1) - OPD(\lambda_2) = [\rho_A(\lambda_1) - \rho_B(\lambda_1)) - (\rho_A(\lambda_2) - \rho_B(\lambda_2)]$$

Source	Reason for OPD-shift	Typical value over 1 mn for K band (m) [(1)]	**Critical time in K band**	Comment
Atmospheric	Turbulence	3E–14	-	Low effect
	Air mass in Delay Line+ $\Delta T(t)$	3 E-11	1 mn	To be monitored
Instrumental Before Spatial Filter	Transmissive dispersion + differential jitter	> 1E-11	< 1 mn	Requires OPD minimization on opto-mechanics + partial calibration with BCD
Spatial Filter	Dispersion in Silica + ΔL (optical fibers) + ΔT		A few hours	To be calibrated with BCD
After Spatial filter	Transmissive dispersion + ΔT	TBD	TBD	Expected to be low (no jitter). Calibrated with BCD
Detector	local variations of chromatic QE and Gain of detector	TBD	TBD	Calibrated with BCD and Spectral Modulation
		[(1)] required : 1.6 e-11 m		

Table 1 lists the different groups of elements to be taken into account (including the atmosphere), together with an estimate of the chromatic OPD values and the expected evolutions with time, to be compared with respect to the calibration procedures.

*Observational procedures and devices for **Calibration / correction** of OPD :*

- slowest effects (time scale ≈5 mn) : **Reference star calibration**

- shorter time scale (about 30 s) : **Spatial modulation with a *beam commuter*** : calibrates all of the chromatic effects occuring from the beam inversion down to the detector. It can be switched much faster than the reference star calibration procedure, thus allowing to get rid of some variations due to the beams jitter.

- **Compensating plates** for the unperfect optics, in order to lower the sensitivity to the VLTI beams jitter.

- **Spectral modulation** : a rotation of the spectral grid shifts the signal of $\Delta\lambda$ in wavelength for calibrating the local variations on the detector (gain and size of pixels, local read-out noise,…)

- **Phase closure** presents a strong potential (Segransan et al, SPIE 2000) for supressing most of the atmospheric and instrumental biases except the chromatic errors on the detector. Phase closure will be available at VLTI at the end of 2002 with ATs and at least at the end of 2003 with UTs.

*Data reduction for* **Calibration / correction** *of OPD :*

Fast effects calibrate from post-observational analysis of spectral dependances.
Assuming the *a prior*i knowledge of a planetary signature parametrized model, the unknown parameters of the model can be constrained together with the unknown biases at a given time by using a fit through simultaneous measurements from separate spectral channels.
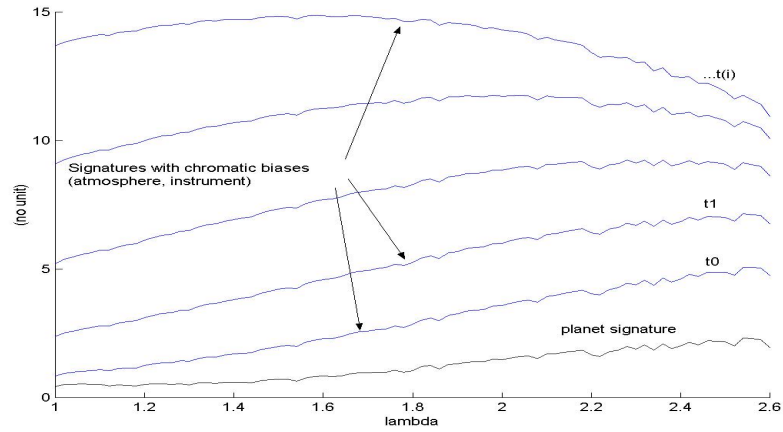
Let $\alpha\_pl(1..n_{pl})$ be the $n_{(pl)}$ independant variables of the signal model, $x\_atm(1..n_{atm})$ and $x\_inst(1..n_{inst})$ the biases originating, respectively, from the atmosphere and the instrument, which affecting the $N_{indep.\ chanels}$ visibility or phase data measured at different λ . We simply have :

If $N_{indep.\ channels} \geq n_{(pl)} + n_{(atm)} + n_{(inst)}$
$\Rightarrow \alpha\_pl(1..n_{pl})$,$x\_atm(1..n_{atm})$, $x\_inst(1..n_{inst})$ determined by a non-linear least-square method

A simple way to figure how the « useful » signal can be discriminated from the pertubations :
The Fourier transform (w.r.t. wavelength) of the atmospheric and instrumental chromatic effects is expected to be higher towards short wavelengths, because of smooth variations of refractive indices with λ :
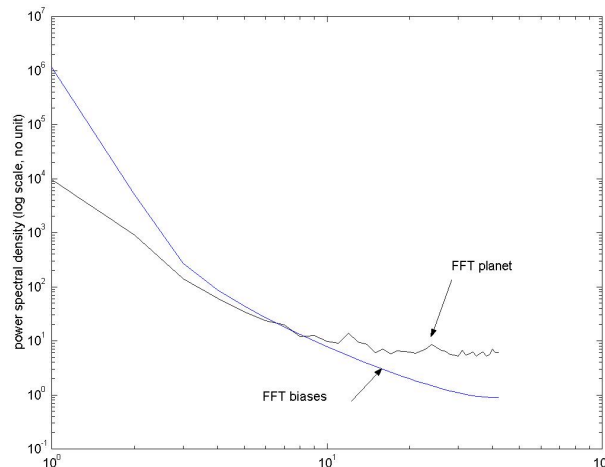
Determining the Angular Diameter of Giant Stars and Planetary Nebulae by Near Infrared Speckle Interferometry

J. Setiawan[1], O. von der Lühe[1], T.R. Bedding[2], A. Zijlstra[3]

[1] Kiepenheuer-Institut für Sonnenphysik, Freiburg (Brsg)-Germany
[2] School of Physics, Sydney-Australia
[3]Department of Physics, The University of Science and Technology, Manchester-U.K

Abstract

We determine the angular diameter of giant stars and planetary nebulae in the near infrared wavelength region (1–2 μm). An infrared camera *SHARP* with a resolution of 0.023 arcsec/pixel was integrated at the *New Technology Telescope* in ESO-La Silla producing speckle interferograms. With the Knox-Thompson cross correlation method we obtained the angular diameter of IK Tau ($59 \cdot 10^{-3}$ arcsec), IRAS 20056+1834 ($63 \cdot 10^{-3}$ arcsec), He 2-113 ($117 \cdot 10^{-3}$ arcsec), and IRAS 07027-3294 ($106 \cdot 10^{-3}$ arcsec). These objects also show the feature of surrounding dust shell around the central stars. Their angular diameters vary from 0.4 to 1.2 arcsec. This technique has been tested on the asteroid Vesta yielding a 529 km of diameter, which is very close to the real average diameter of 525 km, as well as on some bright M giant stars W Hya and R Dor.

keywords: speckle interferograms - Knox-Thompson bispectrum - Wolf-Rayet stars

1. The Knox-Thompson Speckle Interferometry

Since Labeyrie developed a method for an image reconstruction based on computing of the power spectra, which leads to the object's amplitude, the speckle interferometry has been established to be an advantageous tool as an alternative method to the adaptive optics. The main goal of both methods is to reproduce the observed astronomical objects, free from the distorting factors such as the atmospheric turbulences. The reduction works are much easier done in the fourier space, which provides a simple computation for the deconvolution process. Thus, instead of solving the convolution equation:

$$i_n(\vec{x}) = i_0(\vec{x}) \otimes t_n(\vec{x})$$

one has only to do with the multiplication :

$$I_n(\vec{s}) = I_0(\vec{s}) \cdot T_n(\vec{s})$$

where $i(\vec{x})$ is the object's intensity and $t(\vec{x})$ is the *point spread function* (PSF), as well as their fourier transforms $I(\vec{s})$ and $T(\vec{s})$. $T(\vec{s})$ is also called the *moment transfer function* (MTF).

The Knox-Thompson is an easy way to reconstruct the image both in the amplitude and the phase by applying a constant shift $\vec{\Delta}$ to the frequency vector $\vec{s}$.

$$B(\vec{s}, \vec{s} - \vec{\Delta}) = I_0(\vec{s}) \cdot I_0^*(\vec{s} - \vec{\Delta}) \cdot \left\langle T_n(\vec{s}) \cdot T_n^*(\vec{s} - \vec{\Delta}) \right\rangle$$

The quantity $B(\vec{s}, \vec{s} - \vec{\Delta})$ is called the *Knox-Thompson bispectrum*. We mention the fact, that $\left\langle T_n(\vec{s}) \cdot T_n^*(\vec{s} - \vec{\Delta}) \right\rangle$ is real for sufficient great number *n*. The phase of the bispectrum is thus identical to the fourier object's phase. Hence, one may carry an easy computation to determine the object phase by inverting the fourier transformation.

1

2. Image reconstruction

Two targets are usually required for the speckle exposures of point sources and other simple objects. One is the object to be reproduced, the other is a calibrator needed for the deconvolution. In this case numerous objects, e.g. our Sun, make an exception.
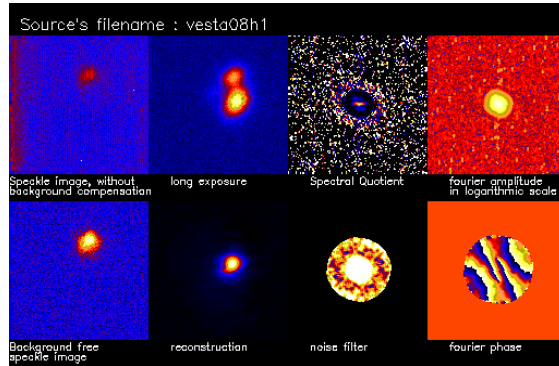
Figure 1.
The figure shows the way from the speckle interferogram (upper left corner) to the pre reconstruction (2nd coloumn, lower panel). The long exposure image is an average image of 500 speckle images.

After subtracting the sky background from the each speckle frame, an averaging by enough number over the entire data set gives the long exposure image. The power spectrum, Knox-Thompson bispectrum and the noise filter are computed with a common fourier analysis. Rewrite the intensity as a complex number:

$$I(\vec{s}) = |I(\vec{s})| \cdot \exp[i\psi(\vec{s})]$$

one may obtain the phase from the equation below:

$$\exp i[\psi(\vec{s}+\vec{\Delta}_k)] = \left[\frac{I(\vec{s}) \cdot I^*(\vec{s}+\vec{\Delta}_k)}{\exp i[\psi(\vec{s})] \cdot |I(\vec{s}) \cdot I(\vec{s}+\vec{\Delta}_k)|}\right]^*$$

The object of interest will have to be deconvoluted with the calibrator by dividing their power spectra in order to eliminate the unknown speckle transfer function $T(\vec{s})$. By building the square root of the 2 dimensional power spectrum, one obtains the visibility function of the deconvoluted image. It is to be fitted with a Bessel function $J_1(x)$ concerning

the *uniform disc* model (UD) or with a gaussian, or a combination of both in order to determine the angular diameter. We prefer the UD model, since the gaussian may result too large value than expected.
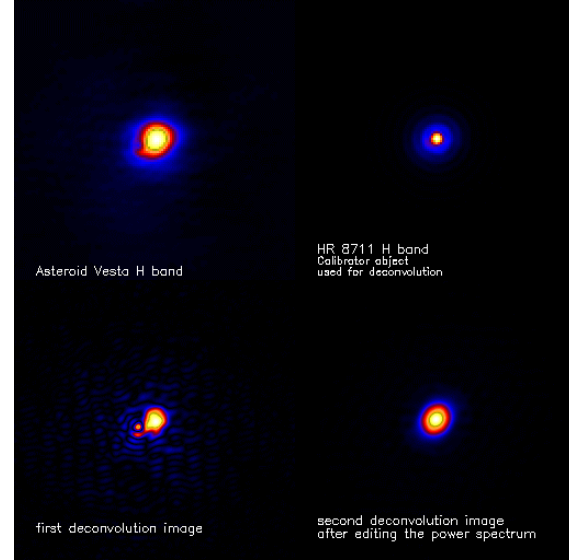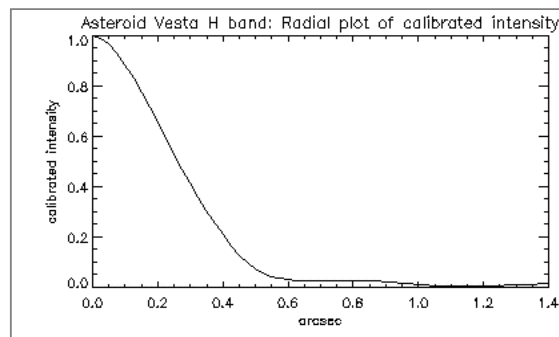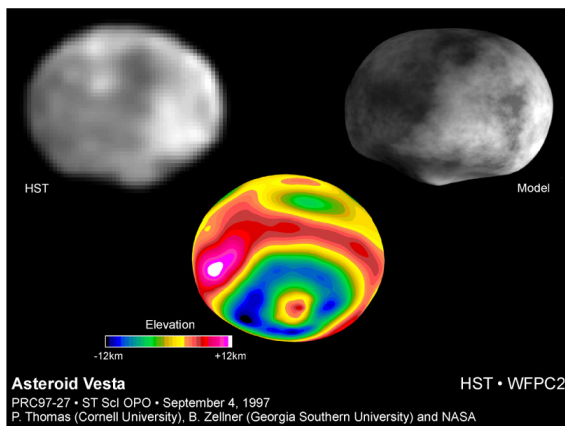

Figure 2.
The pre reconstruction of object will have to be deconvoluted with a calibrator. The first deconvolution shows two resolved objects (see left bottom). The image next to is obtained after cleaning the power spectra from artificial distortions in order to get an easy visibility function to be fitted

3. Test object: asteroid Vesta

A test of the IDL reconstruction package has been carried out by applying the routine to the speckle images of the asteroid Vesta, a well known minor planet. This unique asteroid has been suggested to provide a long record of the evolution of our solar system. The rest of lava streams on its surface observed with the NASA *Hubble Space Telescope* leads to the conclusion, that the asteroid had a melted interior, like the Earth does.
The known average value of the diameter of Vesta is 525 km. In August 1993 by the observation time with the NTT the distance between Vesta and the Earth was approximately 1.3 AU ($\approx 1.95 \cdot 10^8$ km). The angular diameter computed is 559.8 mas, which derives a diameter of 529.3 km. Thus, there is no comparable discrepancy to the known average value mentioned.

Figure 3.
An image of the 525 km diameter asteroid Vesta taken from the NASA Hubble Space Telescope (left).
A radial plot of the calibrated intensity obtained from the speckle reconstruction package (right). An UD model fits the visibility to the value of 0.5598 arcsec, which corresponds to a real diameter of 529.3 km. One may easily compare it with the FWHM shown in the intensity plot.

4. The angular diameters of giant stars

We have successfuly determined the angular diameters of some giant stars: W Hya (HD 120285, M8e), R Dor (HD 29712, M8III), IK Tau (IRAS 03507+1115, M6e), and IRAS 20056+1834 (G0).

W Hya and R Dor are semi regular pulsating stars with the luminosity periods of each 361 and 388 days. Both were observed in 1.45 μm wavelength using a *Circular Variable Filter* (CVF). We computed the average angular diameters of 44.5 mas for W Hya and 55.6 mas for R Dor. The results are in good agreement with the previous measurements (Bedding, von der Lühe, 1993,1995).

The giants IK Tau and IRAS 20056+1834 show the characteristic of dust shell around the massive star. Observations of IK Tau in middle infrared region (11 μm) show periodic shell with radii ranging from 100 mas to 570 mas (Hale,1997). IRAS 20056+1834 is suggested to be a mass-losing supergiant G0 star, which is obscured by a thick dust cloud (Menzies, Whitelock, 1988).
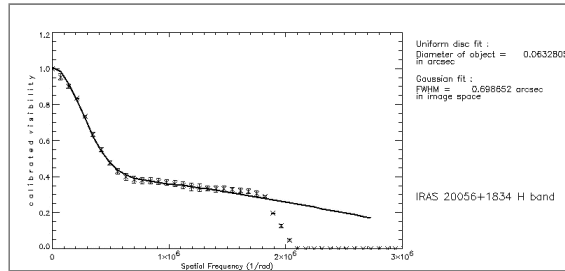
Our observations in H-band result the angular diameter of both the giant stars as follows:

Identifier	core θ [mas]	shell θ[mas]
IK Tau	59±3	410±10
IRAS 20056+1834	63±2	699±30
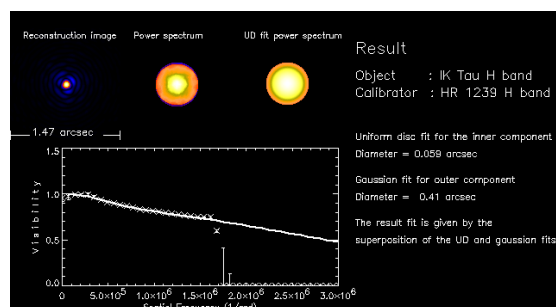
Figure 4.
A chart of the fitting process for the giant star IK Tau. The results vary from 57 to 62 mas for the inner component and from 405 to 420 mas for the outer component (dust shell).

3

Figure 5.
A radial plot of the visibility function of IRAS 20056+1834 exposed in H band (1.6 μm). The prominent gaussian peak clearly shows the existence of the shell around the star. We obtain θ_{UD}= 63±2 mas and θ_{gauss}=699±20 mas.

5. The planetary nebulae around the Wolf Rayet stars He 2-113 and IRAS 07027-7934

We mention, that one of our main problems after the deconvolution is usually caused by the poor quality of the calibrator object. It leaves behind artificial distortions on the power spectrum. An easy way to remove these is by building a suitable mask with a median filter. By subtracting the mask from the origin power spectrum some artificial peaks could be eliminated. Moreover, one should be aware, that this way may reduce the asymmetry information from the original reconstruction, e.g. the shape of "*butterfly wings*" observed on planetary nebulae. This reduction effect can be seen in the reconstruction charts (figure 2 and figure 7). However, since we are only interested in the
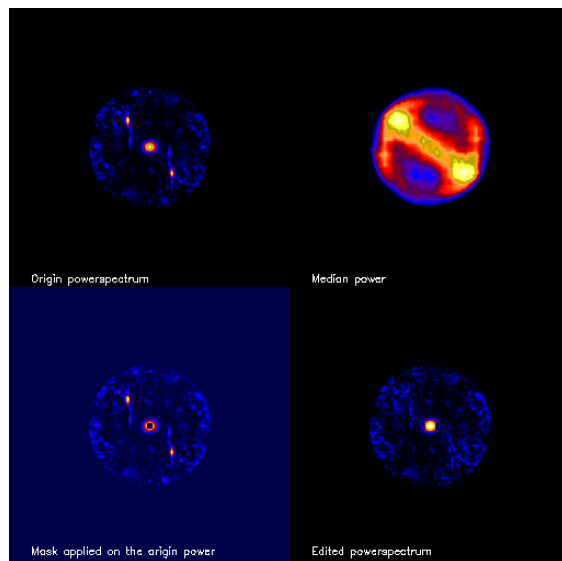
angular diameter, we can use it to obtain a smooth image and a visibility function, which is usually easier to be fitted.

He 2-113 (PN G321.0+03.9) is one of the two WC10 central stars. We resolved this star and the nebula around it in H-band (1.6 μm) by using our simple Knox-Thompson speckle package. Abandoning the shape irregularity of the nebula we computed the angular diameter to be 0.868 arcsec for the nebula and 0.117 arcsec for the central star. As a reference, we also mention, that the nebula was observed with the Hubble Space Telescope in Hβ (4861.3Å). Studies of the Hβ image lead to an angular diameter of 1.4 x 1.1 arcsec^2. This value was obtained by deconvoluting the Hβ images with their [O III] images (de Marco, Barlow, Storey 1998).
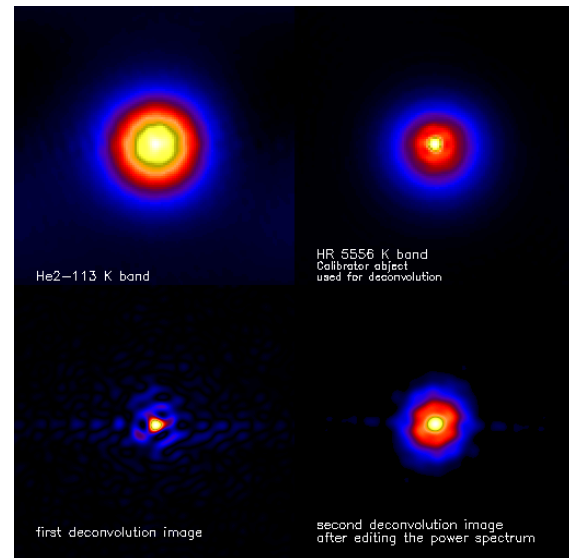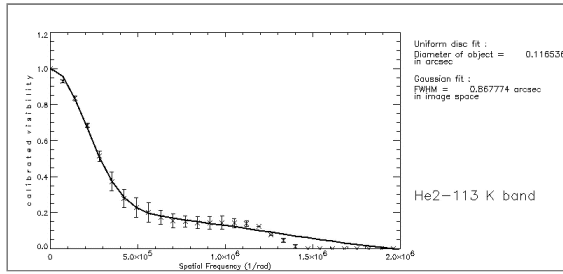

Figure 7.
A reconstruction chart of He2-113 is presented.
The first deconvolution image (lower left corner) still contains artifical distortions, which have to be eliminated by editing the power.
Lower right corner: the image after editing. Indeed it loses the asymmetry information, but it may provide a simple visibility function to make a fit.
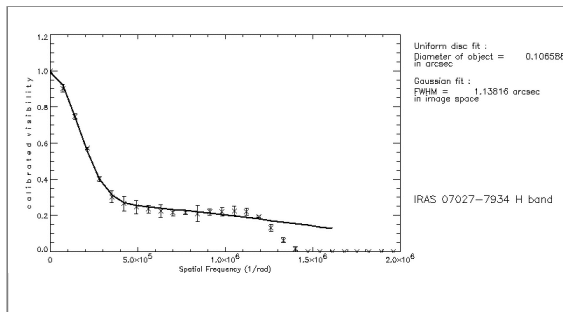

Figure 6.
Upper left: The origin power spectrum shows artificial peaks from unknown sources (either other objects or technical factors). These can cause difficulties in the fitting process. A mask (lower left) is constructed to remove the peaks. The smoothed power spectrum is shown in the lower right corner.

Figure 8.
The fit function of He2-113's visibility (exposed in K band 2.2 μm) yields an angular diameter of θ_{UD}= 117±10 mas (central star), θ_{gauss}=868±50 mas (nebula).

IRAS 07027-7934 (PN G291.3-26.2) was discovered to be a WC11 central star with a young planetary nebula around it (Menzies, Wolstencroft, 1990). From its radial velocity study, the star has been suggested beeing transformed from an oxygen rich star to a carbon rich one during the last 500 years (Zijlstra et al, 1991). We are able to determine the H band angular diameter, but because of the poor quality of the calibrator we can´t fit the diameter of the nebulae in K band. Nevertheless we are able to resolve the central star and give an average fit value of 0.122 arcsec as well as the lower limit of the nebula's diameter.

Identifier		core θ [mas]	shell θ [mas]
He2-113	K	117±10	868±50
IRAS 07027-7934	H	106±8	1138±30
IRAS 07027-7934	K	122±15	>1200

Figure 9.
The visibility function of planetary nebula IRAS 07027-7934 from the speckle exposures in H band. The fitting processes result: θ_{UD} = 106±8 mas and θ_{gauss} = 1138±30 mas

The same way has been attempted to the K band images, but the θ_{gauss} value spreads very large. Nevertheless the lower limit can be determined to be 1200 mas. We derived the θ_{UD} = 122±15 mas for the central star.

6. Conclusion

The angular diameter determination of point sources and other simple objects can be carried out with an easy method such as the Knox-Thompson cross correlation applied to a sufficient number of speckle interferograms. With the appropriated calibration object other components can also be resolved in the reconstruction image. We found out, that the typical value for the angular diameter of point sources in the near infrared wavelength region is ranging from 50 to 100 milli arcsec.

References

Bedding, Zijlstra, von der Lühe: 1997 *MNRAS 286*, 957-962
Bedding, Zijlstra: 1994 *Astron. Astrophys.* 283 955-962
Cohen: 1975 *MNRAS* 173,489-496
De Marco, Barlow, Storey: 1997 *MNRAS* 292, 86-104
De Marco, Barlow, Storey: 1998 *MNRAS* 296, 419-429
Hale et al. 1997: *Astrophysical Journal* 490, p.407
Menzies, Whitelock: 1988 *MNRAS* 233, 697-703
Menzies, Wolstencroft: 1990 *MNRAS* 247, 177-181
Setiawan: graduation thesis (Diplomarbeit, Universität Freiburg 1999)
Zijlstra et al.:1991 *Astron. Astrophys*. 243, L9-L12

5

Expanding shells: instability with non-linear terms

Richard Wünsch, Jan Palouš

*Astronomical Institute, Academy of Sciences of the Czech Republic ,
Boční II 1401, 141 31 Praha 4, Czech Republic*

Abstract. A model of the thin shell expanding into a uniform ambient
medium is developed. Density perturbations are described using equa-
tions with linear and quadratic terms and the linear and the nonlinear
solutions are compared. The interaction of modes on the shell surface is
discussed defining the time when the fragments are formed.

1.   Introduction

The influence of non-linear terms to the fragmentation of expanding HI shells is
discussed extending the linear analysis performed by Elmegreen (1994). We use
the similar approach adopted by Fuchs (1996) who described the fragmentation
of uniformly rotating self-gravitating disks. If some conditions are fulfilled, the
expanding shell may become gravitationally unstable and break to fragments.
Inclusion of higher order terms helps to determine when is the shell fragmented
with better accuracy than the linear analysis the time.

2.   Model used

We consider the cold and thin shell of radius R surrounding the hot interior and
expanding with velocity V into a uniform medium of density ρ_0. The intrinsic
surface density of the shell Σ is composed of unperturbed part Σ_0 plus the
perturbation Σ_1 ($\Sigma = \Sigma_0 + \Sigma_1$). Perturbation Σ_1 results from the flows on the
surface of the shell redistributing the accumulated mass.

We consider angular coordinates $\vec{\Theta} = \vec{x}/R$ and angular velocity $\vec{\Omega} = \vec{v}/R$
to describe the surface of the shell. Hydrodynamical equations are

$$\frac{\partial \Sigma}{\partial t} + 2\Sigma\frac{V}{R} + \Sigma R \nabla \cdot \vec{\Omega} + R\vec{\Omega} \cdot \nabla \Sigma = 0 \; , \tag{1}$$

$$R\frac{\partial \vec{\Omega}}{\partial t} + R^2 \vec{\Omega} \cdot \nabla \vec{\Omega} + V\vec{\Omega} + 3V\vec{\Omega}\frac{\Sigma_0}{\Sigma} = -\frac{c^2}{\Sigma}\nabla \Sigma - \nabla \Phi \tag{2}$$

where c is constant isothermal sound speed, Φ is gravitational potential of the
shell. The second term in the continuity equation and the third and fourth
terms in the equation of motion comes from stretching of the region and from
the accretion of mass. The Poisson equation is:

$$\Delta \Phi = 4\pi G \Sigma \delta(z) \; , \tag{3}$$

2   *Wünsch & Palouš*

where z is a space coordinate perpendicular to the shell surface.

The perturbation of the surface density Σ_1 and of the gravitational potential Φ_1 ($\Phi = \Phi_0 + \Phi_1$) are inserted to these equations and they are Fourier transformed with respect to spatial coordinates. In this way we get the set of equations which describe the evolution of the density and of the velocity field on the surface of the shell.

3.   Linear solution

The linearized version of equations (1)-(3) gives for the most unstable mode the solution also described by Elmegreen (1994):

$$\omega_{\vec{\eta},max}^{(1,2)} = i\frac{3V}{R} \pm \sqrt{-\frac{V^2}{R^2} - \frac{\pi^2 G^2 \Sigma_0^2}{c^2}} \qquad (4)$$

where $\omega_{\eta,max}^{(1,2)}$ is the maximum perturbation growth rate (perturbations of density evolve as $\sim e^{i\omega_\eta t}$). The η_{max} is a dimensionless wavenumber of the most unstable mode of perturbations. If $\omega_{\vec{\eta}}^{(1,2)}$ have got a real part, solution is stable with decreasing oscillations. If not, $\omega_{\vec{\eta}}^{(1)}$ indicates decrease, $\omega_{\vec{\eta}}^{(2)}$ can be imaginary negative and it has meaning of the growth of perturbations, i. e. shell is unstable.

If the shell is unstable, for the certain time, the shell may break to fragments. In Ehlerová et al. (1997) the *fragmentation integral* is defined as:

$$I_{frag}(t) \equiv \int_{t_b}^{t} \omega_{\eta,max}^{(2)}(t')dt' \,, \qquad (5)$$

where t_b is the time when the instability begins. The fragmentation time t_f (the time when the shell is decomposed to fragments) is defined as the time when the fragmentation integral is equal to one:

$$I_{frag}(t_f) = \int_{t_b}^{t_f} \omega_{\eta,max}^{(2)}(t')dt' = 1 \,. \qquad (6)$$

4.   Non-linear analysis

The equations with nonlinear terms are solved by the similar procedure as adopted by Fuchs (1996). We get the set of three ordinary differential equations of the first order describing the evolution of the shell surface density as well as the evolution of the velocity field on the shell surface. The nonlinear terms describe the interaction of the three most unstable modes with wavevectors (of the value η_{max}) inclined at an angle 60°.

The evolution of the maximum perturbation of the surface density is shown in the left panel of Fig (1). The evolution of Σ_1 can be used to define the fragmentation time of the shell. At advanced stages of the fragmentation the value of the maximum perturbation rises steeply with the time and at some time the value of Σ_1 reaches Σ_0. Consequently we define the fragmentation time t_{frag} as the time when $\Sigma_1(t_{frag}) = \Sigma_0(t_{frag})$.

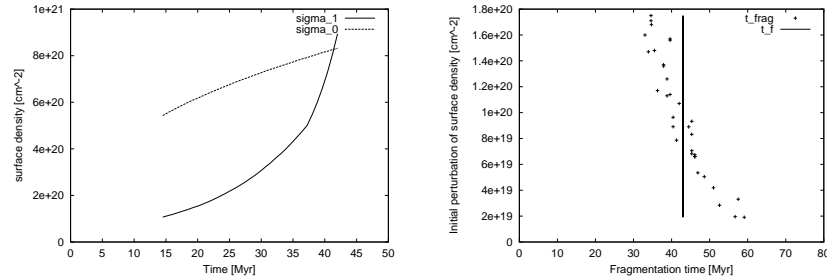*Expanding shells: instability with non-linear terms*   3

Figure 1.   Left panel: The time evolution of Σ_0 and Σ_1. Right panel: Dependence of t_{frag} on a value of the initial perturbation of the surface density. The solid line gives the time defined by the fragmentation integral (6).

     In the right panel of Fig (1) the dependence of t_{frag} obtained from the solution of the non-linear equations on the value of the initial perturbation is shown. t_{frag} may be compared to the fragmentation time t_f obtained from the linear analysis defined with the fragmentation integral (6).

5.   Conclusions

An interaction of three modes of the type discussed by Fuchs (1996) occurs on the shell surface. The time when fragments form depends on initial conditions. If the initial perturbation of surface density is of the order $\sim 10^{19} - 10^{20}\ cm^{-2}$, which is a typical value of inhomogeneities in the ISM, the average value of fragmentation time t_{frag} is approximately of the same value as the time t_f when the fragmentation integral (6) is equal to 1, with a spread of $\pm 10\ Myr$ depending on the value of the initial perturbation.

References

Ehlerová, S., Palouš, J., Theis, Ch., Hensler, G. 1997, A&A, 328, 121
Elmegreen, B. G. 1994, ApJ, 427, 384
Fuchs, B. 1996, MNRAS, 278, 985

RADIATION-DRIVEN DISKONS
Alexander V. Serber, Novgorod Institute of Applied Physics

Abstract

We overview the formation and structure of extended plasma envelopes formed in white dwarf magnetospheres under the action of radiation pressure at cyclotron frequencies and discuss possible observation evidences of such peculiar objects called radiation-driven diskons.